

# An orbital release model for the Orion BN/KL fingers

A. C. Raga<sup>1\*</sup>, P. R. Rivera-Ortiz<sup>2</sup>, J. Cantó<sup>3</sup>, A. Rodríguez-González<sup>1</sup>

A. Castellanos-Ramírez<sup>3</sup>

<sup>1</sup> *Universidad Nacional Autónoma de México, Instituto de Ciencias Nucleares, AP 70-543, CDMX 04510, México*

<sup>2</sup> *Observatoire de Grenoble, Grenoble Alpes, CNRS, IPAG, 38000 Grenoble, France*

<sup>3</sup> *Universidad Nacional Autónoma de México, Instituto de Astronomía, AP 70-264, CDMX 04510, México*

## ABSTRACT

We present a simple model in which the bullets that produce the “Orion fingers” (ejected by the BN/KL object) are interpreted as protoplanets or low mass protostars in orbit around a high mass star that has a supernova explosion. As the remnant of the SN explosion has only a small fraction of the mass of the pre-supernova star, the orbiting objects then move away in free trajectories, preserving their orbital velocity at the time of release. We show that a system of objects arranged in approximately co-planar orbits results in trajectories with morphological and kinematical characteristics resembling the Orion fingers. We show that, under the assumption of constant velocity motions, the positions of the observed heads of the fingers can be used to reconstruct the properties of the orbital structure from which they originated, resulting in a compact disk with an outer radius of  $\sim 2.4$  AU.

**Key words:** stars: winds, outflows – ISM: jets and outflows – ISM: individual objects: Orion BN/KL

## 1 INTRODUCTION

One of the more intriguing flows in the Galactic ISM is composed of the “fingers” radiating away from the Orion BN/KL object (a massive embedded stellar object surrounded by a compact nebula, see Becklin & Neugebauer 1967 and Kleinmann & Low 1967). These fingers were first reported by Allen & Burton (1993) in IR H<sub>2</sub> and [Fe II] emission, and have lengths of up to  $\sim 2'$  ( $\sim 7 \times 10^{17}$  cm at a distance of 400 pc). The bases of these fingers, as well as a multitude of other filaments are detected in interferometric CO observations (Zapata et al. 2009; Zapata et al. 2017; Bally et al. 2017). The CO emission of the individual fingers shows a remarkable “Hubble law” of linearly increasing radial velocities with distance from the BN/KL object.

Doi et al. (2002) and Bally et al. (2011, 2015) obtained proper motions of the IR line emission of the heads of the “Orion fingers”, and Nissen et al. (2007) obtained radial velocities of these features. Nissen et al. (2012) combined proper motion and radial velocity measurements to obtain the full spatial motion of some of the fingers.

The fact that the motions of the heads of the individual fingers give similar dynamical timescales implies that they were all ejected in an “explosive” event of short duration. This result stands regardless of the fact that some of the

“bullets” at the tips of the fingers might have had a substantial slowing down along their trajectories (Rivera-Ortiz et al. 2019a, b).

It has been proposed that this sudden event could have been:

- a result of the breakup of a multiple stellar system (see Reipurth et al. 2010; Reipurth & Mikkola 2012, 2015; Moeckel & Goddi 2012). The dynamics of a 3- or 4-body system can explain the high velocities of the stars near the BN/KL object (observed in radio continuum by Rodríguez et al. 2005 and by Gómez et al. 2005, 2008), and in principle could trigger the “interstellar bullets” that create the Orion fingers. A first attempt to model the ejection of a cluster of bullets through a gravitational interaction was recently presented by Rivera-Ortiz et al. (2021),

- a result of a supernova, which could liberate the bound orbital motion of companion stars into free hyperbolic orbits. This scenario can explain the high velocities of the stars around BN/KL, and could as well result in the ejection of the observed high velocity bullets.

These scenarios are discussed in the previous literature on the Orion fingers (see, e.g., Bally et al. 2011, 2017 and Zapata et al. 2017).

A remarkable feature of the outflow from BN/KL is that while the whole system of fingers shows an elongated morphology towards the NW and SE, this roughly bipolar

\* E-mail: raga@nucleares.unam.mx

structure does not correspond to a division between blue and redshifted emission. There is a “red/blueshift” division in the system of fingers, but with respect to an axis roughly aligned with the NW/SE elongation. This NE/SW division of the blue (NE) and redshifted (SW) emission is clearly seen in Figure 3 of Zapata et al. (2017). However, there are some filaments with the “wrong radial velocity shift” (i.e., some redshifted filaments to the NE and some blueshifted filaments to the SW), as can be seen in the observations of Bally et al. (2017).

In the present paper we show that the elongated morphology and “side-to-side” red/blue shifted kinematics of the system of Orion fingers can be straightforwardly explained as the free propagation of a system of objects with a planar initial velocity distribution. In section 2 we show how this extremely simple model produces spatial and radial velocity distributions that qualitatively resemble the system of Orion fingers. Section 3 derives the relation between the radial (position) distribution function and the orbital velocity distribution of a system of massless particles in circular orbits around a massive object. In section 4 we show how under the assumption of a planar velocity distribution and free post-supernova trajectories the observed positions (and also velocity information if available) can be used to reconstruct the velocity distribution of the bullet system. In section 5 we use the observed positions of the tips of the Orion fingers to reconstruct their velocity distribution and the radial position distribution of the bullets on the pre-release circumstellar disk. The results are discussed in section 6.

## 2 INSTANTANEOUS RELEASE MODEL

### 2.1 General considerations

We assume that we have a system of  $N$  non-interacting particles with initial (at  $t = 0$ ) positions  $\underline{x}_{0,i}$  and velocities  $\underline{v}_i$  (with  $i = 1, \dots, N$ ). For  $t > 0$ , the free particles then have (vector) positions:

$$\underline{x}_i(t) = \underline{x}_{0,i} + t\underline{v}_i. \quad (1)$$

If initially the particles lie within a volume of size  $L$ , it is clear that for  $t \gg L/v_m$  (where  $v_m$  is the smallest modulus of all of the particle velocities) the first term on the right hand side of equation (1) can be neglected, and we have trajectories that are independent of the initial positions of the particles, and only depend on their initial velocities.

We present two examples of this trivial model, a “thin disk” (S 2.2) and a “thick disk” initial distributions (§2.3). The thin disk distribution has a system of particles in coplanar circular orbits around a central star, and the thick disk distribution has circular orbits with a range of inclinations of their orbital axes. At  $t = 0$  the central star has a supernova explosion, ejecting most of its mass: a remnant of only  $\sim 2 M_\odot$  will be left behind when a  $\sim 30 M_\odot$  solar metallicity star has a SN explosion (see. e.g., Liu et al. 2021 and references therein). With such a drastic decrease in the mass of the central star, the orbiting particles will suddenly find themselves in free, very open hyperbolic orbits, which can be approximated as linear trajectories.

The question then is what are these particles in initial circular orbits around the pre-supernova, massive star: obvious candidates are giant planets/protoplanets and/or very

low mass stars forming in a disk around the massive star. This gives the attractive picture of the Orion fingers being produced by ejected pre-planetary or pre-stellar condensations.

### 2.2 Planar distribution with circular orbits

We now consider a planar distribution of 100 massless particles orbiting around a central star of mass  $M_*$ , with orbital radii  $r$  distributed randomly in the  $0 \rightarrow R_0$  range. The phase of the orbit at  $t = 0$  is chosen uniformly in the  $0 \rightarrow 2\pi$  range. Their orbital velocities then are:

$$v_{orb} = v_0 \sqrt{\frac{R_0}{r}}, \quad (2)$$

with

$$v_0 \equiv \sqrt{\frac{GM_*}{R_0}}. \quad (3)$$

The combination of  $v_0$  and  $R_0$  gives a characteristic time

$$t_0 \equiv \frac{R_0}{v_0} = \sqrt{\frac{R_0^3}{GM_*}}. \quad (4)$$

For example, for a distribution of particles with an outer radius  $R_0 = 100$  AU orbiting around a central star with a  $M_* = 30M_\odot$  mass, we have  $v_0 = 16.3$  km s $^{-1}$  and  $t_0 = 29.1$  yr.

Assuming that at  $t = 0$  the central star suddenly “disappears”, the particles then evolve with straight trajectories, preserving their initial velocity. Figure 1 shows the particle trajectories up to a time  $300 t_0$ , projected onto the plane of the sky for four different assumed angles between the disk axis and the line of sight.

### 2.3 Non-planar distribution with circular orbits

We now consider the same problem of 100 massless particles in initial circular orbits (which are “liberated” at  $t = 0$ , see §2.2), but allowing the individual orbits to have axes with random tilts in the  $0 \rightarrow 35^\circ$  range with respect to the average disk axis.

The resulting particle trajectories at  $t = 300 t_0$  (see equation 4) are shown in Figure 2. We see that the variation in the initial orbital axes of the particles results in a partial mixing of redshifted and blueshifted particles above/below the  $y' = 0$  axis. This effect is more strongly pronounced at the smaller and larger values of the inclination ( $i = 5$  and  $85^\circ$ , see Figure 2).

## 3 THE RELATION BETWEEN THE RADIAL DENSITY AND VELOCITY DISTRIBUTIONS OF PARTICLES IN AN ORBITAL DISK

In §2.2 we considered a set of  $N$  particles in co-planar circular orbits around a central source, with a uniform radial distribution. Let us now look at a more general problem, in which the radial particle distribution has an arbitrary power law form:

$$f(r) = \frac{(\alpha + 1)N}{R_0^{\alpha+1}} r^\alpha, \quad (5)$$

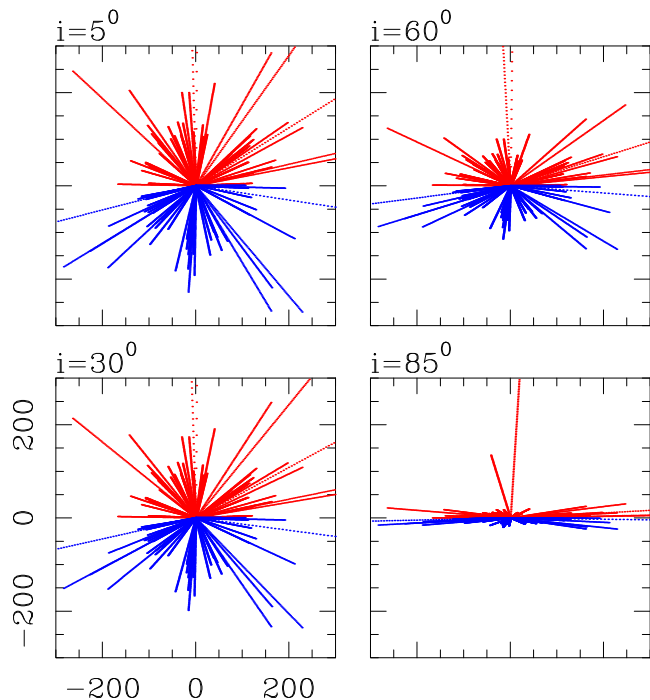


**Figure 1.** Trajectories of a system of free particles originating from a thin disk of outer radius  $R_0$  and outer orbital velocity  $v_0$  released at  $t = 0$  and ending at  $300t_0$  (see the text). The four frames show the projected trajectories for 4 different values of the inclination of the initial orbital axis with respect to the line of sight. The colours of the trajectories correspond to positive (red) and negative (blue) radial velocities of the ejected particles. The  $(x', y')$  plane of the sky axes are labelled in units of  $R_0$ .

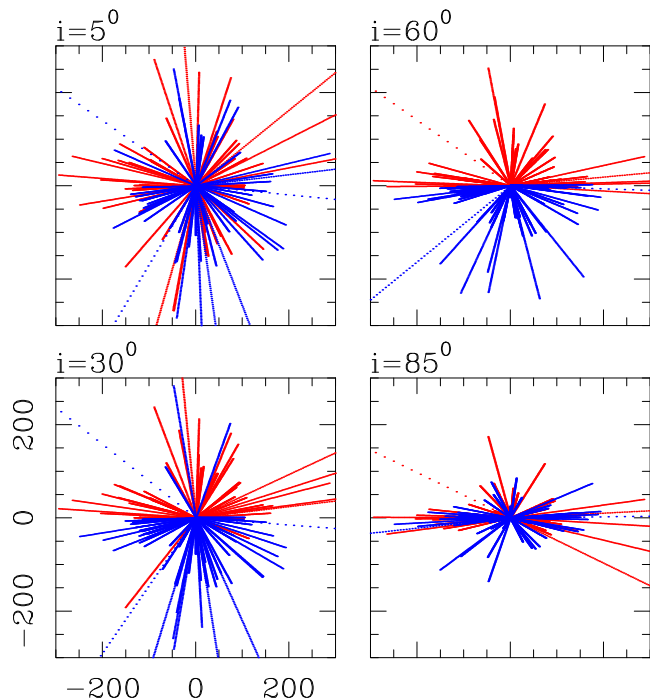


**Figure 2.** The same as Figure 1 but for an initial “thick disk” distribution of orbits with axes with random tilts of up to  $35^\circ$  with respect to the disk axis.

where the proportionality constant is determined from the  $\int_0^{R_0} f(r)dr = N$  condition, with  $r$  being the radius on the orbital plane and  $R_0$  being the radius of the outer orbit of the  $N$  particles.

It is straightforward to show that this distribution corresponds to a surface number density of particles:

$$n(r) = \frac{(\alpha + 1)N}{2\pi R_0^{\alpha+1}} r^{\alpha-1}. \quad (6)$$

As the particles are in circular orbits, their velocity as a function of  $r$  is given by equation (2). We can then calculate the distribution  $g(v)$  of the modulus  $v$  of the velocities of the particles as:

$$g(v) = \frac{f(v)}{|dv/dr|} = \frac{2(\alpha + 1)Nv_0^{2+2\alpha}}{v^{3+2\alpha}}, \quad (7)$$

where equations (2) and (5) have been used for the second equality. For the case of a uniform radial particle distribution (with  $\alpha = 0$ ) described in §2.2, this gives

$$g(v) = \frac{2Nv_0^2}{v^3}. \quad (8)$$

## 4 RECONSTRUCTING THE ORBITAL DISK FROM THE EVOLVED TRAJECTORIES

### 4.1 The ballistic trajectories

We now consider the ballistic trajectories of particles at large times, when they have reached distances  $L \gg R_0$ , where  $R_0$  is the size of the original disk around a star that at  $t = 0$  became a SN, thus releasing the particles from the central, stellar potential. For  $t \gg t_0$  (see equations 1 and 4), the trajectory of a particle is:

$$x(t) = tv \cos \theta; \quad y(t) = tv \sin \theta, \quad (9)$$

where  $\theta$  is the (random) angle between the orbital velocity and the  $x$ -axis and  $v$  is modulus of the orbital velocity of one of the particles.

If we assume that the initial disk is at an inclination  $i$  with respect to the line of sight (with the  $y$ -axis into and the  $x$ -axis on the plane of the sky), the plane of the sky trajectory will be:

$$x'(t) = x(t); \quad y'(t) = y(t) \cos i. \quad (10)$$

The parcel has plane of the sky velocities

$$v_{x'} = v \cos \theta; \quad v_{y'} = v \sin \theta \cos i, \quad (11)$$

a radial velocity (with positive values away from the observer)

$$v_r = v \sin \theta \sin i, \quad (12)$$

and a proper motion velocity

$$v_{pm} = v \sqrt{\cos^2 \theta + \sin^2 \theta \cos^2 i}. \quad (13)$$

Finally, from equation (11) we compute the average value over all bullets of the moduli of  $x'$  and  $y'$ :

$$\begin{aligned} \langle |x'| \rangle &= t \langle v \rangle \langle |\cos \theta| \rangle; \\ \langle |y'| \rangle &= t \langle v \rangle \langle |\sin \theta| \rangle \cos i, \end{aligned} \quad (14)$$

where we have assumed that  $v$  and  $\theta$  are uncorrelated. Also,  $\langle |\cos \theta| \rangle = \langle |\sin \theta| \rangle = 2/\pi$  for random directions on a plane.

## 4.2 The reconstruction

We assume that at a time  $t \gg t_0$  we observe the positions of a system of particles arising from an orbital disk system that at  $t = 0$  lost its central gravitational binding source. We assume that we have the plane of the sky positions for  $N$  observed “bullets”. If for these bullets we have observed proper motions and radial velocities, we can directly calculate the distribution function of the velocity moduli of the ensemble of particles.

If we have the radial velocities  $v_r$  and/or the proper motions  $v_{pm}$  for only some of the bullets (the proper motion of at least one bullet being necessary), using the assumption that the motions lie on a plane (i.e., the plane of an initial orbiting disk structure), we can still reconstruct the velocity distribution function. To this effect, we proceed with the following steps:

- *Step 1:* If the observed system lends itself to an interpretation as an “unbound debris disk”, we should observe a clear side-to-side division between positive and negative radial velocities (see Figure 1). The line on which the radial velocities change sign defines the  $\theta = 0$  direction, and then the  $(x', y')$  coordinates correspond to the distances along and across this axis (respectively), with the origin located at the point of divergence of the particle trajectories.

- *Step 2:* We then use the bullets for which we have observed proper motions to calculate the time  $t$  since the gravitational release through the relation  $t = \sqrt{x'^2 + y'^2}/v_{pm}$ , which (apart from being evidently correct) is obtained from equations (9), (10) and (13). For an instantaneous release model to be appropriate, similar values of  $t$  should be obtained for all of the bullets with observed proper motions.

- *Step 3:* We now calculate the averages of the moduli of the plane of the sky  $(x', y')$  coordinates over all bullets (which we call  $\langle |x'| \rangle$  and  $\langle |y'| \rangle$ , respectively) and use equation (14) to find the inclination angle as:

$$i = \cos^{-1} \left( \frac{\langle |y'| \rangle}{\langle |x'| \rangle} \right). \quad (15)$$

- *Step 4:* With the computed values of  $t$  and  $i$ , we now use the relation:

$$v = \frac{|x'|}{t} \sqrt{1 + \frac{y'^2}{x'^2 \cos^2 i}}, \quad (16)$$

to calculate the full velocity  $v$  for all of the individual observed bullets (equation 16 can be directly obtained from equations 9-10). These velocities can be appropriately binned to obtain the empirical distribution function  $g_e(v)$  of the velocities of the particles.

## 5 RECONSTRUCTION OF THE VELOCITY DISTRIBUTION OF THE ORION FINGERS

We took the dataset of Bally et al. (2011, see their Figure 1), who analyse two epochs of  $H_2$  images to obtain the positions and proper motions of the Orion finger bullets. We then followed the procedure described in §4:

- *Step 1.* From the CO radial velocities of Zapata et al. (2009, their Figure 1), we see that the change of sign in the radial velocities lies at a  $52^\circ$  angle (measured W from N).

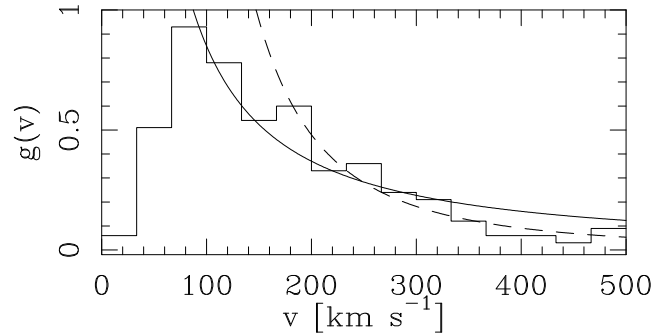


**Figure 3.** The histogram shows the velocity distribution function deduced from the observed positions of the tips of the Orion fingers. The solid and dashed curved show the power law fits to the observed distribution function in the  $v \geq 80$  and  $v \geq 180$   $\text{km s}^{-1}$  velocity ranges (respectively).

We then calculate the  $(x', y')$  coordinates of  $N = 168$  bullets (with  $x'$  along the change of sign axis).

- *Step 2.* We can obtain  $t$  from the positions and proper motion velocities of the bullets with Eq. (15). Most of the resulting ages are below 1000 years, and we assumed a representative age of 500 yr, equal to the dynamical age of the protostellar objects around Orion BN/KL (see Rodríguez et al. 2005).

- *Step 3.* We calculate the average values  $\langle |x'| \rangle$  and  $\langle |y'| \rangle$  of the moduli of the coordinates, and use equation (15) to obtain  $i = 71^\circ$ .

- *Step 4.* We calculate the moduli of the velocities of all particles with equation (16), and group them in  $33 \text{ km s}^{-1}$  wide bins to obtain the empirical velocity distribution function  $g_e(v)$  (normalized so that  $\int g_e(v) = N$ , where  $N = 168$  is the number of bullets in our sample). The resulting velocity distribution function is shown in Figure 3.

The velocity distribution has a steep rise with increasing velocities, peaks at  $v \approx 80 \text{ km s}^{-1}$ , and then has an approximately monotonic decrease for larger  $v$  (see Figure 3). The initial rise in  $g_e(v)$  probably corresponds to incompleteness in the data set, as a multitude of short, low radial velocity filaments are present in the CO data (see, e.g., Bally et al, 2017), and are not seen in  $H_2$  images.

Because of this, we carry out power law fits of the form

$$g(v) = B \left( \frac{200 \text{ km s}^{-1}}{v} \right)^\beta, \quad (17)$$

to the empirical  $g_e(v)$  setting a lower velocity cutoff  $v_{min}$  for the fit. We have tried two values for this cutoff:

- (i)  $v_{min,1} = 80 \text{ km s}^{-1}$ , corresponding to the peak of the empirical  $g_e(v)$ ,

- (ii)  $v_{min,2} = 180 \text{ km s}^{-1}$ , where the decrease of  $g_e(v)$  shows an inflection.

As we can see in Figure 3, the first fit clearly does not reproduce the decrease of the observed distribution  $g_e(v)$  at velocities  $> 300 \text{ km s}^{-1}$ . For this reason, we favour the second fit, which does not reproduce the low velocity behaviour of  $g_e(v)$ , but this can be understood as being a result of an incompleteness in the sample of the shorter, lower velocity filaments and/or of a physical “soft cutoff” of the distribution at lower velocities.

With this second fit (see the dashed line of Figure 3), we obtain  $B = (0.48 \pm 0.03) \text{ km}^{-1}\text{s}$  and  $\beta = 2.36 \pm 0.22$  (see equation 17). Using equations (7) and (17) we see that the exponent of the corresponding initial radial distribution of the bullets (see equation 5) is  $\alpha = (\beta - 3)/2 = -0.32 \pm 0.02$ . Also, comparing equations (7) and (17), from our fit we obtain a velocity  $v_0 = (106 \pm 13) \text{ km s}^{-1}$  at the outer edge of the initial disk. We should note that for calculating this velocity we used the  $N = 168$  number of bullets in our sample, which probably has a substantial incompleteness. If we assume that the disk had a pre-supernova central star of  $30 M_{\odot}$ , this outer edge velocity implies a disk radius of  $\sim 2.4 \text{ AU}$ .

## 6 CONCLUSIONS

In a recent paper, Dempsey et al. (2020) modeled the propagation of orbital debris (protoplanets and/or planets) dispersed during the breakup of a multiple stellar system. We study a similar scenario, in which the planets or protoplanets orbit an embedded massive, pre-supernova star, and travel in approximately straight trajectories (preserving the modulus of their orbital velocity) when the supernova ejects most of the stellar mass. This scenario has no problem in reproducing the high velocities (of up to  $\sim 500 \text{ km s}^{-1}$ ) observed in the Orion fingers.

We argue that:

- the elongated morphology and the division across the elongation axis into red and blueshifted regions of the ensemble of fingers can be trivially explained as the free expansion of an approximately planar, orbital disk structure,
- the velocity distribution of the heads of the Orion fingers implies a minimum orbital velocity of  $\sim 100 \text{ km s}^{-1}$ , and therefore a maximum radius of  $\sim 2.4 \text{ AU}$  (for an assumed  $30 M_{\odot}$  mass for the pre-supernova star).

From the observed velocity distribution we find that the initial radial distribution of objects is approximately  $\propto r^{\alpha}$ , with  $\alpha \sim -0.3$ . This corresponds to a surface density of objects with a power law exponent of  $\sim -1.3$ .

An interesting point is that there is currently no evidence of the existence of exoplanets or protoplanets orbiting massive stars or protostars. Possibly the Orion fingers are evidence in favour of their existence? They imply the presence of  $\sim 100$ - $200$  condensations within a few AU from the star! A larger size for the initial disk structure is of course possible if a substantial outwards acceleration of the condensations (i.e., the protoplanets) occurs when they interact with the expanding supernova ejection.

We should finally mention that two other systems of “radiating fingers” have been detected in our Galaxy: DR 21 (Zapata et al. 2013, with only a few bullets) and G5.89 (Zapata et al. 2020, a system comparable to the Orion fingers). Based on these three detections, Zapata et al. (2020) conclude that these “multi-fingered explosive events” have a frequency that is similar to the supernova rate of our galaxy. This result also indicates that our model deserves further study.

## ACKNOWLEDGMENTS

AR and ARG acknowledge support from the PAPIIT (UNAM) project IA103121. PRO acknowledges funding from the European Research Council (ERC) under the European Union’s Horizon 2020 research and innovation program, for the Project “The Dawn of Organic Chemistry” (DOC), grant agreement No. 741002. ACR acknowledges support from a DGAPA-UNAM postdoctoral fellowship.

Data availability: No new data were generated or analysed in support of this research.

## REFERENCES

- Allen, D. A., & Burton, M. G. 1993, *Nature*, 363, 54A  
 Bally, J., Cunningham, N. J., Burton, M. G. et al. 2011, *ApJ*, 727, 113  
 Bally, J., Ginsburg, A., Arce, H., et al. 2017, *ApJ*, 837, 60  
 Becklin, E. E., & Neugebauer, G. 1967, *ApJ*, 679, L121  
 Dempsey, R., Zakamska, N. L., & Owen, J. E. 2020, *MNRAS*, 495, 1172  
 Doi, M., O’Dell, C. R., & Hartigan, P. 2002, *AJ*, 124, 445  
 Gómez, L., Rodríguez, L. F., Loinard, L., et al. 2005, *ApJ*, 635, 1166  
 Gómez, L., Rodríguez, L. F., Loinard, L., et al. 2008, *ApJ*, 685, 333  
 Kleinmann, D. E., Low, F. 1967, *ApJ*, 149, L1  
 Liu, T., Wei, Y.-F., Xue, L. & Sun, M.-Y. 2021, *ApJ*, 908, 106L  
 Moeckl, N., & Goddi, C. 2012, *MNRAS*, 419, 1390  
 Nissen, H. D., Gustafsson, M., Lemaire, J. L., et al. 2007, *A&A*, 466, 949  
 Reipurth, B., Mikkola, S., Connelley, M., et al. 2010, *ApJL*, 725, L56  
 Reipurth, B., & Mikkola, S. 2012, *Nature*, 492, 221  
 Reipurth, B., & Mikkola, S. 2015, *AJ*, 149, 145  
 Rivera-Ortiz, P. R., Rodríguez-González, A., Cantó, J., & Zapata, L. A. 2021, *ApJ*, in press (arXiv:2106.01283)  
 Rivera-Ortiz, P. R., Rodríguez-González, A., Hernández-Martínez, L., & Cantó, J. 2019a, *ApJ*, 874, 38  
 Rivera-Ortiz, P. R., Rodríguez-González, A., Hernández-Martínez, L., et al. 2019b, *ApJ*, 885, 104  
 Rodríguez, L. F., Poveda, A., Lizano, S., & Allen, C. 2005, *ApJ*, 627, L65  
 Zapata, L., Loinard, L., Schmid-Burgk, J., et al. 2011, *ApJ*, 726L, 12Z  
 Zapata, L., Schmid-Burgk, J., Pérez-Goytia, N., et al. 2013, *ApJL*, 765, L29  
 Zapata, L., Schmid-Burgk, J., Rodríguez, L. F., et al. 2017, *ApJ*, 836, 133  
 Zapata, L., Ho, P. T. P., Fernández-López, M., et al. 2020, *ApJL*, 902, 47

This paper has been typeset from a  $\text{\TeX}/\text{\LaTeX}$  file prepared by the author.